AAPS PharmSciTech, Vol. 19, No. 7, October 2018 (© 2018)
DOI: 10.1208/s12249-018-1031-2

Research Article

Theme: Team Science and Education for Pharmaceuticals: the NIPTE Model
Guest Editors: Ajaz S. Hussain, Kenneth Morris, and Vadim J. Gurvich

A Simplified Geometric Model to Predict Nasal Spray Deposition in Children and Adults

Mow Yee Foo,[1,2] Namita Sawant,[1] Ellen Overholtzer,[1] and Maureen D. Donovan[1,3]

Received 3 March 2018; accepted 24 April 2018; published online 11 June 2018

Abstract. A mathematical approach was developed to estimate spray deposition patterns in the nasal cavity based on the geometric relationships between the emitted spray plume and the anatomical dimensions of the nasal valve region of the nasal cavity. Spray plumes were assumed to be spherical cones and the nasal valve region was approximated as an ellipse. The effect of spray plume angle (15–85°) on the fraction of the spray able to pass through the nasal valve (deposition fraction) was tested for a variety of nasal valve (ellipse) shapes and cross-sectional areas based on measured dimensions from pediatric and adult nasal cavities. The effect of the distances between the tip of the nasal spray device and the nasal valve (0.2–1.9 cm) on the deposition fraction was also tested. Simulation results show that (1) decreasing spray plume angles resulted in higher deposition fractions, (2) deposition fraction was inversely proportional to the spray distance and the nasal valve (ellipse) major/minor axis ratio, and (3) for fixed major/minor axis ratios, improved deposition occurred with larger nasal valve cross-sectional areas. For a typical adult nasal valve, plume angles of less than 40° emitted from a distance of 1 cm resulted depositions greater than 90% within the main nasal cavity, whereas for a 12-year-old child, only the most narrow plume angles (< 20°) administered resulted in significant deposition beyond the nasal valve.

KEY WORDS: airway modeling; intranasal delivery; nasal spray; nasal deposition; nasal valve.

INTRODUCTION

Understanding nasal deposition patterns resulting from nasal sprays or other intranasal dosage forms is an important aspect in the development of effective nasally administered drug products, including vaccines, agents for topical action, or agents utilizing the nasal mucosa as an entry portal to the systemic circulation. Early nasal deposition models developed for use in the fields of inhalation toxicology and industrial hygiene were derived based on the behavior of a series of suspended, mono-disperse aerosols with known inertial (d_A^2Q) and diffusional parameters ($D^{-0.5}Q^{-0.125}$) without assuming any initial aerosol particle trajectory, velocity, or limiting airway geometry (1). Unfortunately, the difference between these models and the conditions present when using sprays emitted from nasal administration devices limit the utility of the inhalation toxicology models for use in estimating deposition of spray droplets into the nasal cavity. The deposition of nasal sprays depends on the nasal airway geometry as well as the spray properties (2,3). Most previous spray deposition models have been focused on adult nasal cavity dimensions, yet it is well understood that children have smaller nasal airways compared to adults (4), and the development of models capable of predicting spray deposition patterns in different populations with variations in nasal airway dimensions is needed to improve the formulation development process for nasal spray dosage forms.

The deposition of nasal sprays delivered from mechanical pump spray devices has been studied, both *in vitro* and *in vivo*, in children and adults, in order to identify the key factors required for efficient intranasal delivery (5–8). Regardless of the experimental methodology, most sprays were observed to impact in the anterior regions of the nasal cavity with very little spray able to penetrate deep into the turbinate region of the main nasal cavity (9–12). Kublik and Vidgren provided a review of the nasal deposition literature and concluded that the anatomical constraints of the nasal cavity caused most inhaled particles to deposit in the region of the nasal valve due to either the physical constriction of the airway passage or the increase in airflow resistance present in

Guest Editors: Ajaz S. Hussain, Kenneth Morris, and Vadim J. Gurvich

[1] College of Pharmacy, University of Iowa, 115 S. Grand Ave., Iowa City, Iowa 52242, USA.
[2] *Present Address:* Novartis Pharmaceuticals, Shanghai, China.
[3] To whom correspondence should be addressed. (e–mail: maureen-donovan@uiowa.edu)

that region. For any particles or droplets that are able to pass through the nasal valve region, most deposit directly on the anterior surfaces of the turbinates which impinge directly into the path of the airstream (13). Quantitatively, the proportion of a spray which impacts in the anterior region of the nose/nostril region has been reported to be between 20 and 80% (14) and, in some cases, was shown to exceed 90% of the administered dose (2,15), resulting in limited amounts of the dose administered actually reaching the intended administration site.

Recently, investigators have begun to use nasal cavity dimensions derived from MRI and CT images coupled with computational fluid dynamic (CFD) modeling techniques to study particle deposition in the extrathoracic airways (2,9,16–18). Kimbell et al. incorporated droplets with specific trajectories and spray parameters into a CFD model to simulate spray deposition patterns within the nasal cavity (2), and showed that post-nasal valve particle deposition was improved when either smaller droplet sizes or slower spray velocities were used. Inthavong et al. also showed a similar dependence on particle size and velocity, which aerodynamically was expressed as the particle Stokes number (16). While CFD is an extremely powerful technique, its use to guide specific formulation and device selection is unlikely to gain wide acceptance due to the need for significant computing resources to perform each simulation.

Abd El-Shafy et al. (19) introduced a simpler, geometric approach to predict spray deposition efficiency by comparing the ratio of the areas of a circular nasal valve region relative to the area of the circular base of the emitted spray cone which forms when the spray cone intersects with the plane of nasal valve. This model provided reasonably accurate predictions of the fraction of a spray cone (spray plume) reaching the turbinate region of the nasal cavity—the target region for most nasally administered drug products. An enhanced model has been derived with the intention to improve the accuracy of the El-Shafy approach and to expand the application of the geometric models to evaluate the deposition of nasal sprays in children in addition to adults. Geometric models emphasize the importance of nasal valve dimensions, spray emission distance, and spray plume characteristics and do not require sophisticated modeling/simulation software. A geometric model can be used to estimate the fraction of a spray which will deposit in the main nasal cavity, predict the differences in deposition due to varying nasal valve dimensions, and provide a rational basis for device design, particularly for spray tip length and spray plume characteristics. The enhanced geometric model described in this report can be used to quickly identify formulation and spray device combinations that can provide desired deposition patterns in target populations and can be used to evaluate whether specific formulation-device combinations may need to be developed for some populations.

METHODS

Model Development

Atomization, dispersion of the bulk liquid contained in a reservoir into droplets suspended in a gaseous phase, takes ~ 100–200 ms to complete after actuation of a nasal spray device. The process of atomization usually produces a continuous flow of polydisperse droplets with an array of trajectories emitted from the spray orifice. The emitted droplets form a three-dimensional, inverted spherical cone whose vertex extends from the device tip. The dimension of the spray cone (plume) angle is defined by the outermost boundaries of the droplet trajectories generated during atomization. While spray plume characteristics may vary during the atomization process, they are treated as static quantities in the development of this geometric model. A spherical cone, which is also equivalent to a segment of a sphere, was used to approximate the geometry of a spray plume, and the deposition fraction (DF) in the turbinate region was defined as the fraction of the upper spherical surface area of the emitted cone which penetrated through the nasal valve (Fig. 1).

$$DF = \frac{\text{UpperSurface Area(past nasal valve)}}{\text{UpperSurface Area(emitted cone)}} \quad (1)$$

Geometrically, there are two equivalent ways to estimate the DF: (i) the volume fraction of a spherical cone (spray plume) which passes through the nasal valve or (ii) the fraction of the surface area of a spherical cone centered at the source that corresponds to the spray paths which pass through the nasal valve. These approaches are essentially equivalent since a sphere of radius, r, has a volume of $(4/3)\pi r^3$ and a surface area of $4\pi r^2$. Thus, every unit of surface area

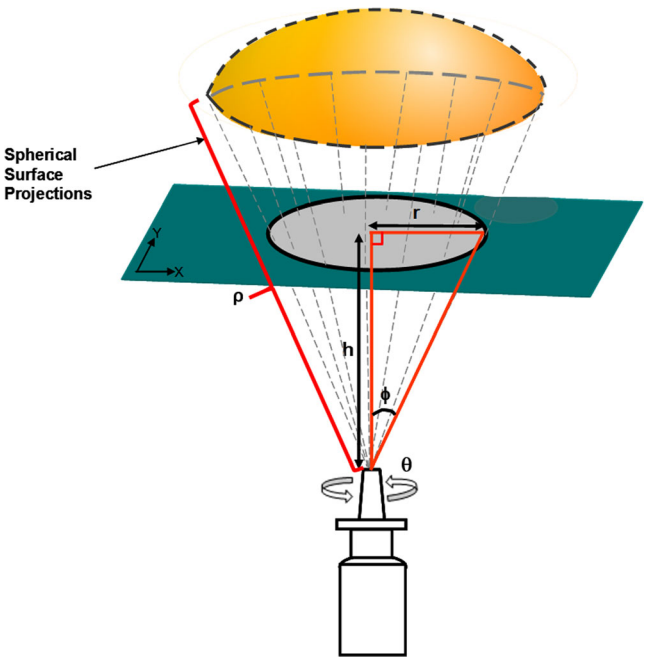

Fig. 1. Projection of a segment of spherical surface area (SA) with a radius (ρ) from an intersection through a horizontal plane with a radius (r) at a distance (h) from the spray device tip with half plume angle (ϕ) and a rotation angle (θ). This projection simulates a nasal spray passing through the nasal valve (circular area) and entering the turbinate region of the main nasal cavity. The spherical surface area that contacts the nasal turbinates is proportional to the function of the spray plume passing through the nasal valve

corresponds to exactly (r/3) units of volume. Any difference between the two approaches is mathematically eliminated by evaluating the deposition as the ratio of the emitted plume and the plume which passes through the nasal valve. For simplicity in computation, the current model was developed using the spherical surface area approach.

The spherical cone proposed in the model is assumed to be a homogenous object. Preliminary studies undertaken to test this assumption showed that, while the droplet size distribution was somewhat variable throughout a nasal spray plume, the normalized droplet mass concentration was equal among various segments of the plume (20).

Shape of the Spray and the Nasal Valve

Since the emitted spray is assumed to be in the shape of a spherical cone (spherical segment), in spherical coordinates its volume (V) is described by $\int_0^{2\pi}\int_0^{\phi}\int_0^{\rho}\rho^2\sin\phi d\rho d\phi d\theta$ (21) where ρ is the radius of the sphere (spherical cone), ϕ is the half plume angle between the two outermost boundaries of the spray cone, and θ is the rotation angle perpendicular to the plane of the spray cone (Fig. 1). The upper surface area (SA) of the spherical cone can be defined by Eq. 2 (22):

$$SA = \int_0^{2\pi}\int_0^{\phi}\rho^2\sin\phi d\phi d\theta = 2\pi\rho^2(1-\cos\phi) \tag{2}$$

When the cone points vertically, its intersection with a horizontal plane is a circle. Any region on the surface of the spherical cone can be projected from the horizontal plane by integrating the perimeter of the intersecting horizontal region (Fig. 1). For a point on the plane of intersection in polar coordinates (r,θ), the differential $d\theta$ of the spherical cone is equivalent to $d\theta$ on the plane, and since $\phi = \tan^{-1}(r/h)$ (Fig. 1), then $d\phi = \frac{dr}{(r/h)^2+1}$. The projection of such a region from the plane onto the sphere has area (Eq. 3):

$$\begin{aligned} SA_{\text{proj}} &= \iint_{\substack{\text{projected}\\ \text{region}}} \frac{\rho^2\sin\phi}{(r/h)^2+1} drd\theta \\ &= \iint_{\text{region}} \frac{\rho^2(r/h)}{\left((r/h)^2+1\right)^{(3/2)}} drd\theta \end{aligned} \tag{3}$$

Changing to rectangular coordinates, where $rdrd\theta = dydx$, Eq. 4 becomes:

$$SA_{\text{proj}} = \iint_{\substack{\text{projected}\\ \text{region}}} \frac{\rho^2}{h\left(\frac{x^2+y^2}{h^2}+1\right)^{3/2}} dydx \tag{4}$$

The nasal valve is a somewhat elliptically shaped opening in the nasal cavity with a narrow minor axis that limits the amount of spray able to penetrate into the main nasal cavity. For modeling purposes, the nasal valve was assumed to be a perfect ellipse. The nasal valve has been reported to be at a distance of 2–2.5 cm from the nostril opening in adults (4,23,24). When the spray device is inserted ~1 cm into the nostril, it is reasonable to approximate the distance between the spray device tip and the nasal valve to be ~1 cm. Based on this, the spray distance value (h) was fixed at 1 cm for initial modeling purposes. Other situations can be easily accommodated, however, for alternate values of h. The final projection area is defined by:

$$SA_{proj} = \iint_{\substack{projected\\ region}} \frac{dydx}{(x^2+y^2+1)^{(3/2)}} \tag{5}$$

Modeling Spray Deposition

Depending on the spray plume angle (2ϕ), there are three scenarios which could be anticipated relative to the dimensions of the nasal valve. For these scenarios, ϕ_{major} (Fig. 2a) is defined as the hypothetical half angle that extrapolates from a fixed distance source to the edge of the nasal valve major axis. Similarly, ϕ_{minor} (Fig. 2a) is the hypothetical half angle that extrapolates from a fixed distance source to the edge of the nasal valve minor axis.

Case I: Entire Spray Cone Passes Through the Ellipse ($2\phi_{spray} < 2\phi_{minor}$)

When the minor axis of the elliptical nasal valve is greater than the diameter of the circular region of the spray cone's intersection with the plane of the nasal valve (Fig. 2b), the entire spray cone passes through the nasal valve with a deposition fraction equal to 1.

Case II: Spray Cone Angle Is Greater than the Major Axis of Ellipse ($2\phi_{spray} \geq 2\phi_{Major}$)

In this case, the DF can be represented by the area of the elliptical nasal valve's projection onto the spherical segment relative to the original spherical cone's surface area, (Eq. 7). The term $(2-2\cos\phi)\pi$ was obtained from Eq. 2 for the value $\rho = 1$ (Fig. 2c). The x and corresponding y coordinates for each point on the perimeter of the elliptical region in the plane can be defined as $[x, \pm b(1-x^2/a^2)^{1/2}]$ (Fig. 2c) and, thus, the DF can be described by Eq. 7:

$$SA = \int_{-a}^{a}\int_{-b\sqrt{1-x^2/a^2}}^{b\sqrt{1-x^2/a^2}} \frac{dydx}{(x^2+y^2+1)^{(3/2)}} \tag{6}$$

$$DF = \frac{\int_{-a}^{a}\int_{-b\sqrt{1-x^2/a^2}}^{b\sqrt{1-x^2/a^2}} \frac{dydx}{(x^2+y^2+1)^{(3/2)}}}{(2-2\cos\phi)\pi} \tag{7}$$

Case III: When ($2\phi_{minor\ axis} \leq 2\phi_{spray} \leq 2\phi_{major\ axis}$)

If the major axis of the ellipse is wider than that of the spray cone, but the minor axis is not, the resulting points of intersection (Fig. 2d) can be described by substituting the

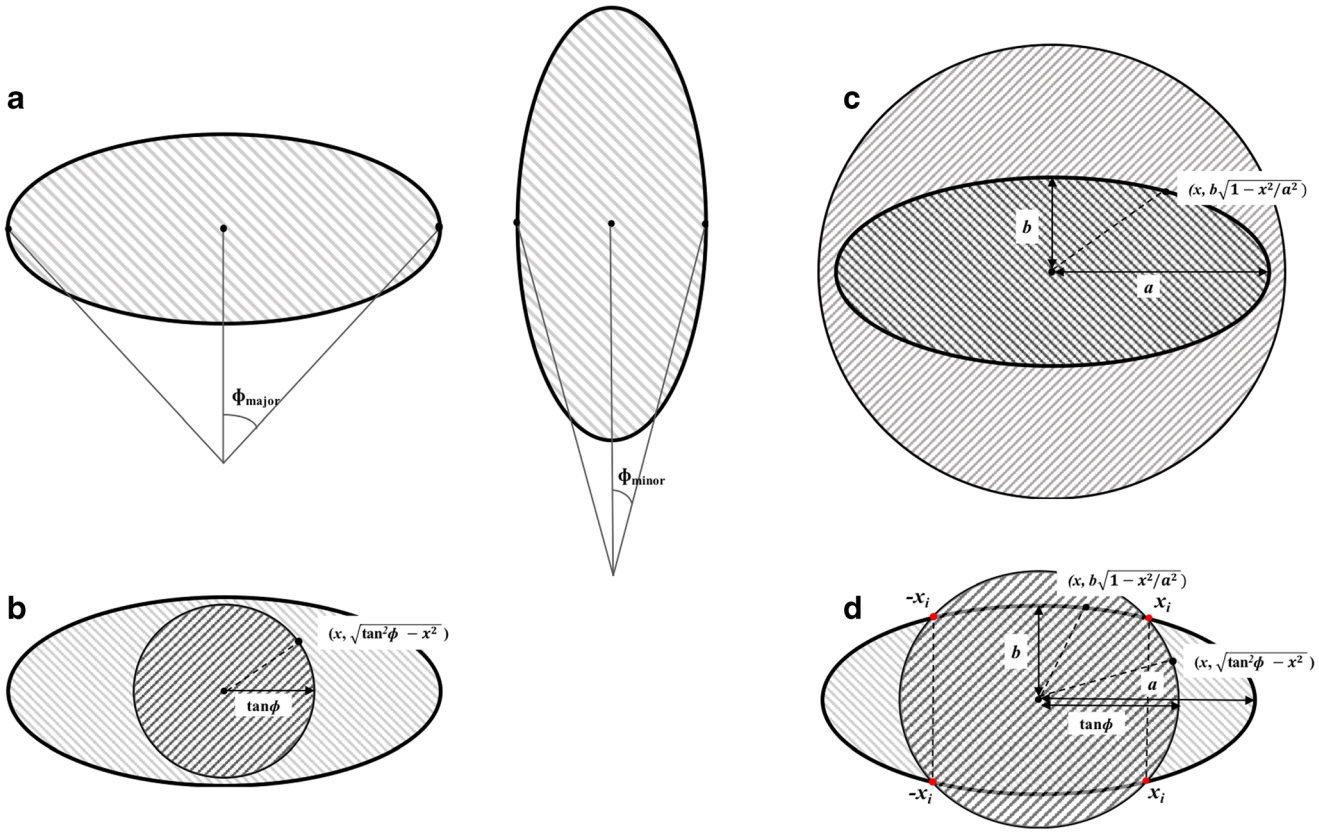

Fig. 2. Two-dimensional illustration of the intersection between a spherical spray cone on the horizontal plane of the nasal valve (ellipse). The cross-hatched region denotes the overlapping region between the spray cone (circular region, forward slash) and the nasal valve (back slashed region). Labels between each arrow denote the distance from the point of origin in rectangular coordinates. **a** ϕ_{major} is the hypothetical half angle that extrapolates from a fixed distance source to the edge of the nasal valve major axis and ϕ_{minor} is the hypothetical half angle that extrapolates from a fixed distance source to the edge of the nasal valve minor axis. **b** Spray cone passes through the nasal valve completely resulting a circular intersection on the plane ($2\phi_{spray} < 2\phi_{minor}$). **c** Spray cone intersects completely with the nasal valve perimeter resulting an elliptical intersection on the plane ($2\phi_{spray} > 2\phi_{major}$). **d** Spray cone intersects at points (x_i) that have a distance between the major and minor axes lengths of the nasal valve resulting in a partial elliptical and partial circular intersection on the plane ($2\phi_{minor} \le 2\phi_{spray} \le 2\phi_{major}$)

equation of an ellipse (Eq. 8) into that for a circle (Eq. 9) resulting in Eq. 10:

$$x_i^2/a^2 + y_i^2/b^2 = 1 \tag{8}$$

$$x_i^2 + y_i^2 = \tan^2\phi \tag{9}$$

Therefore, x_i, the intersection of the x-axis coordinate for the ellipse and circle, is:

$$x_i = \sqrt{\frac{\tan^2\phi - b^2}{1 - b^2/a^2}} \tag{10}$$

The portion of the spray cone passing through this ellipse is given by evaluating the projection integral for the ellipse from $x = -x_i$ to $x = x_i$, with the corresponding y coordinate defined by the dimension of the ellipse ($\pm b\sqrt{1-x^2/a^2}$). The projection integral for the remaining regions derived from the circular shape of the spray cone is evaluated from $x = x_i$ to $x = \tan\phi$ and from $x = -\tan\phi$ to $x = -x_i$ with the corresponding y coordinate defined by the dimension of circle ($\pm\sqrt{\tan^2\phi - x^2}$). Due to symmetry, we can evaluate the positive x values and multiply the result by 2. The total projection areas relative to the original spherical cone's surface area, $(2 - 2\cos\phi)\pi$ obtained from Eq. 2 for $\rho = 1$, can be calculated using Eq. 11.

$$DF = 2\left[\frac{\int_0^{x_i}\int_{-b\sqrt{1-x^2/a^2}}^{b\sqrt{1-x^2/a^2}} \frac{dydx}{(x^2+y^2+1)^{(3/2)}} + \int_{x_i}^{\tan\phi}\int_{-\sqrt{\tan^2\phi - x^2}}^{\sqrt{\tan^2\phi - x^2}} \frac{dydx}{(x^2+y^2+1)^{(3/2)}}}{(2-2\cos\phi)\pi}\right] \tag{11}$$

Deposition fraction simulations were conducted for each of the cases described. Spray plume angles ranging between 15° and 85° were evaluated at 5° intervals, and simulations were carried out using the nasal valve dimensions representative of adults as well as a range of children ages (infants to 12 years old). Based on reported nasal valve cross-sectional areas, a value of 0.7 cm^2 (2,25) was used as a representative adult nasal valve area and 0.2 cm^2 (4,26–28) was used as a representative pediatric nasal valve area in the current simulations. A nasal valve major/minor axis ratio of 2.4 equivalent to major axis (0.725 cm) and minor axis (0.3 cm) of the reference nasal valve cast described by Foo was used for adults (20). Likewise, a nasal valve major/minor axis ratio of 10 was used for children, based on the major axis

(0.79 cm) and minor axis (0.079 cm) measured from a 12-year-old child's nasal cast (12).

Test Scenario I: Effect of Major/Minor Axis Ratio

For adults, a fixed nasal valve area of 0.7 cm^2 (2,25) with 11 sets of major/minor axis ratios ranging from 1 to 9.7 was evaluated, whereas for children a fixed nasal valve area of 0.2 cm^2 (4,26–28) with five sets of major/minor axis ratios ranging from 4 to 12 was used. The major/minor axis ratios range used for the adult nasal cavity dimensions (1 to 9.7) represented the transition from a circle to an elongated ellipse (Fig. 3(A)) and also included 2.4, the major/minor axis ratio measured from an adult nasal cast (20). Major/minor axis ratios ranging from 4 to 12 represented an elliptical-shaped nasal valve and also bracketed the major/minor axis ratio 10, measured from a pediatric nasal cast (12). The plume angles used in the simulation ranged from 15° to 85°, which includes typical plume angles observed from most nasal spray devices.

Test Scenario II: Effect of Nasal Valve Area

A fixed major/minor axis ratio of 2.4 with nine sets of nasal valve cross-sectional areas ranging from 0.1 to 1.15 cm^2 representative of the adult nasal cavity was used. A fixed major/minor axis ratio of 10 with four sets of cross-sectional areas ranging from 0.1 to 0.4 cm^2 was used as representative of various pediatric nasal valve areas.

Test Scenario III: Effect of Device Insertion Depth

In addition to the nasal valve area and major to minor axis ratio, another factor which could potentially affect spray deposition is the actuation distance between the device tip and the nasal valve (Fig. 3(C)). During actual patient use, different insertion distances or spray tip lengths/designs may change the distance within the nostril region available for spray plume development and could potentially alter the deposition fraction. For this test scenario, the nasal valve area and dimension were fixed for both adult (major axis = 0.725 cm and minor axis = 0.3 cm (ratio = 2.4); area = 0.7 cm^2) and pediatric (major axis = 0.79 cm and minor axis = 0.079 cm (ratio = 10); area = 0.2 cm^2) subjects. Spray distances of 0.2 to 1.9 cm were simulated for plume angles between 15° and 85°.

Each combination of variables was substituted into the appropriate case scenario Eqs. 6, 8, or 12 and evaluated numerically using Scientific WorkPlace 5.0 (MacKichan Software, Poulsbo, WA) and Maple 2017 (Maplesoft, Waterloo, ON Canada). The output DF results were used to construct contour and three-dimensional response surface plots using SigmaPlot 13.0 (Systat Software, San Jose, CA) for visualization and analysis.

RESULTS

Model Evaluation

The deposition efficiencies of various formulations were tested using several different commercially available nasal spray devices in an elliptically shaped nasal valve model with a major/minor axis ratio = 2.4 and area = 0.7 cm^2 (20). A range of spray plume angles was obtained by varying the glycerin/water formulations sprayed from the devices. A good statistical correlation ($r^2 = 0.9503$) was obtained between the experimental results and those predicted by the spherical cone model described in this report (Fig. 4). Further examination of the spherical cone model compared to the previous flat cone described by Abd El-Shafy et al. (19) shows that the spherical cone model is able to predict the deposition of a wide variety of sprays experimentally measured using an elliptical nasal valve model.

Test Scenario I: Fixed Nasal Valve Area with Different Major/Minor Axis Ratios

For a constant plume angle, the model predicted deposition fraction (Fig. 5) was reduced when the major/minor axis ratio of the ellipse increased. This implies that a circular nasal valve shape (major/minor axis ratio = 1) results in the highest fractional turbinate deposition while further elongation of the ellipse (nasal valve) leads to lower deposition efficiencies due to a greater loss of the spray outside of the minor axis (Fig. 5a, b). As is evident from Fig. 5c, d, even lower deposition fractions were predicted for an ellipse-shaped nasal valve using the small cross-sectional area (0.2 cm^2) observed for children. Additionally, the increase in the ellipticity of the nasal valve had minimal effect on deposition efficiencies of spray plumes wider than 60° for a fixed cross-sectional area of 0.2 cm^2, since the majority of the volume of these wide plumes pass around/outside of the area of the ellipse, regardless of its specific dimensions.

Test Scenario II: Fixed Major/Minor Axis Ratio with Different Nasal Valve Cross-Sectional Areas

Simulations predicted that deposition efficiency increased with increasing nasal valve cross-sectional area for all plume angles (Fig. 6). This finding is intuitive since a larger orifice should allow a higher fraction of the spray cone to pass. However, it should be noted that the deposition efficiency was extremely sensitive to plume angle for the small nasal valves present in children. This can be clearly illustrated by observing the drastic decrease in predicted deposition efficiency from 100 to 50% for plume angles between 15° and 40° ($\Delta = 25°$) when the nasal valve cross-sectional area was 0.2 cm^2, compared to the need for a 40° change in plume angle for a similar magnitude decrease for an adult nasal valve area of 0.7 cm^2 (Fig. 5a–d). Deposition fractions were significantly lower for a larger major to minor axis ratio (10) and smaller cross-sectional area (0.2 cm^2) characteristic of the nasal valve regions of children compared to those in adults. For example, a plume angle of 15° predicted a 100% deposition for all nasal valve areas with a 2.4 (adult nasal cavity) major/minor axis ratio (Fig. 6a, b), whereas the same plume angle predicted only 50 to 90% deposition efficiency for the children's small and more ellipse-shaped nasal valves (Fig. 6c, d).

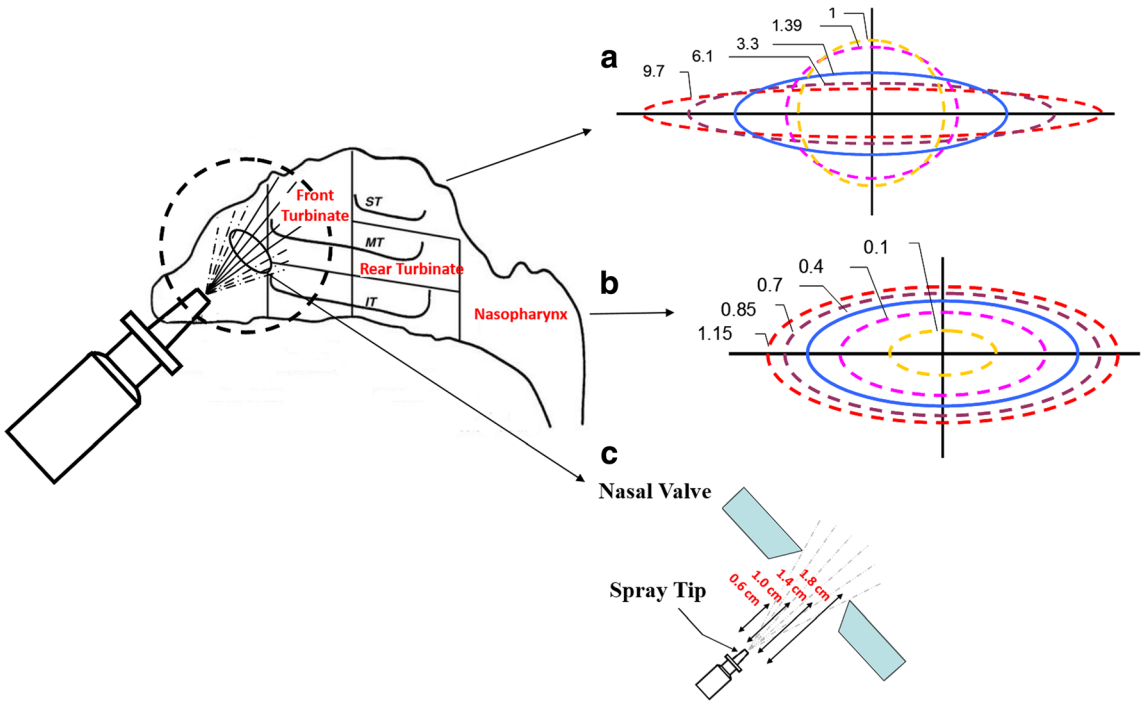

Fig. 3. Schematic representation of a nasal spray device inserted into the nostril and aligned perpendicular to the nasal valve with diagrammatic representations of the conditions used for simulations. **a** Nasal valve with a fixed cross-sectional area (0.7 cm^2) with varying major to minor axis ratios (1–9.7). **b** Nasal valve with a fixed major to minor axis ratio (2.4) with varying cross-sectional areas (0.1–1.15 cm^2). **c** Fixed nasal valve cross-sectional area (0.7 cm^2) and a fixed major to minor axis ratio (2.4) with varying distance between the spray device and the nasal valve

Test Scenario III: Fixed Nasal Valve Area and Major/Minor Axis Ratio at Different Spray Distances

The model predicts that the plume angle required for a 100% deposition efficiency decreased as the distance between the device tip and the nasal valve increased (Fig. 7). If a spray was actuated in close proximity to the adult nasal valve, full deposition past the nasal valve could still be accomplished, even for wide plume angles, but much narrower plume angles were required when the distance from the nasal valve increased beyond 0.5 cm. For example, 100% deposition efficiency was maintained for plume angles $\leq 80°$ when an actuation distance of 0.4 cm was used, but 100% deposition efficiency could be maintained for actuation distances as great as 1.7 cm for sprays with 20° plume angles (Fig. 7a, b). The predicted deposition fractions were significantly lower at all actuation distances for the 12-year-old pediatric nasal cavity. The small area and elliptical shape of nasal valve resulted in decreased deposition fractions compared to adults (Fig. 7a, b), and only plume angles $< 40°$ with actuation distances < 0.5 cm from the nasal valve resulted in near 100% deposition past the nasal valve (Fig. 7c, d).

DISCUSSION

The validity of the spherical cone model described in the current study was evaluated by comparing experimental results obtained from an adult human nasal cast to the model predicted results along with an additional comparison to the results predicted using the Abd El-Shafy et al. model based on a circular-shaped nasal valve of exactly same cross-sectional area as that of the current spherical cone model (19). Good agreement between the spherical cone model predictions and the experimentally measured

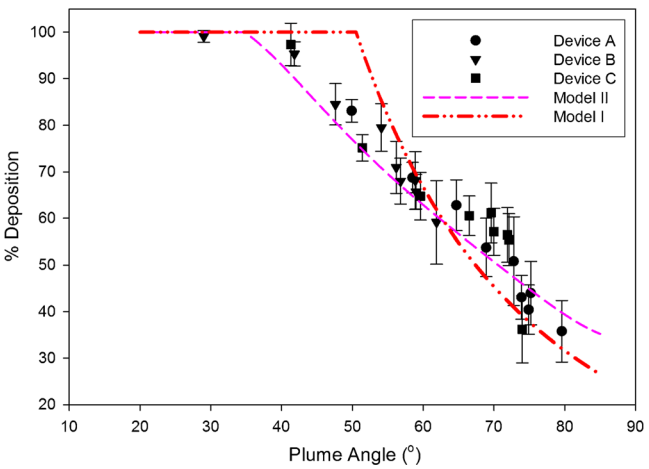

Fig. 4. Comparison of two simulated deposition profiles with experimentally obtained deposition efficiency data. Model I reported by Abd El-Shafy et al. (19). $\left[\%D = \frac{A}{\pi(Pw)^2} \times 100\right]$ where $\%D$ = delivery efficiency, A = area of nasal valve, and Pw = plume width obtained at a fixed distance from the spray tip to nasal valve which incorporated a fixed circular nasal valve of 0.7 cm^2 using a flat cone model. Model II describes the spherical cone model using an elliptical nasal valve with cross-sectional area of 0.7 cm^2 and major/minor axis ratio of 2.4, and a spray distance of 1 cm. Experimental data (devices A, B, C) were obtained using an elliptically shaped nasal valve model with a 0.7-cm^2 nasal valve cross-sectional area (20)

deposition results confirms the ability of this model to accurately predict post-nasal valve deposition from different spray devices emitting a broad range of plume angles and droplet sizes based on elliptical-shaped approximation of the nasal valve (Fig. 4) (6).

In vitro experiments have also been conducted using a nasal cast derived from a 12-year-old child to study the deposition pattern of nasal sprays in children compared to adults (12). The 12-year-old child's nasal cast was segmented in five sections, and the second section contained the nasal valve (~ 0.2 cm^2 cross-sectional area) and the anterior portion of the turbinate region. Experimental results showed that for plume angles > 26°, deposition occurred primarily in the anterior sections of the nasal cast, with minimal transfer of the spray into the turbinate region of the child's nasal cavity. As demonstrated in Fig. 6c, d, the predicted fraction of a spray passing through the nasal valve (0.2 cm^2 cross-sectional area) is < 0.4 for plume angles greater than 26° and far less than 0.4 as the area of the nasal valve region is decreased (12).

Since, regardless of spray characteristics, most of the spray droplets which pass through the nasal valve enter the main nasal cavity and impact on the anterior surface of the inferior turbinate without penetrating further into the cavity, focusing on the spray characteristics that determine spray penetration through the nasal valve allows for much simpler experimental or theoretical systems to be used to predict deposition efficiency. These simplified models allow the easy prediction of the fractional deposition of a nasal spray beyond the nasal valve and increase the ability to rapidly design or select spray devices for optimized turbinate deposition based simply on the plume geometry, device tip length, and typical nasal cavity dimensions when the remaining spray parameters, such as droplet size and speed, are held within typical ranges produced by current spray devices.

In order to evaluate nasal deposition patterns using *in silico* simulations, a geometric approach was used and a simulation model was developed based on a simplifying assumption of an elliptically shaped nasal valve. In reality, the nasal valve has an arbitrary shape which is not fully represented by either a circle, an ellipse, or a triangle and, to some extent, appears somewhat as an inverted "comma" shape in the adult. In addition, the simplest version of the geometric model presumes that the spray forms a right cone where the center ray from the apex of the cone impacts perpendicularly on the plane of the nasal valve (Fig. 1). Fixing the spray emission to be perpendicular to the plane of the nasal valve allows for the prediction of the highest possible fraction of the spray plume able to pass directly through the nasal valve; other administration angles will only serve to decrease the efficiency of deposition. Since the geometric model was developed to provide rapid predictions of maximal turbinate region deposition, limiting the impact angle at the nasal valve to 45° provides a useful initial deposition target value for rapid evaluation of spray/nasal cavity/user variable interactions.

The simulation results show that deposition patterns in children are far more sensitive to plume shape and device insertion depth than those in adults. Deposition fractions decreased as the ellipticity of the nasal valve (major/minor axis) increased in both children and adults. Longer and narrower nasal valves provide greater barriers to the passage of nasal sprays due to the extremely narrow minor axis dimension. Only sprays with narrow plume angles (< 30° in adults and < 20° in children) are able to deposit significant amounts of the spray droplets in the turbinate region of the main nasal cavity. The small overall cross-sectional area of the children's nasal valves also severely limits the post-nasal valve deposition of any nasal spray. The deposition efficiency in both adults and children could be improved by actuating the spray device in close proximity to the nasal valve. This requires the insertion of the nasal spray device deeply into the nostril, however, and that may be associated with discomfort by many users and may actually be impossible in very young children if the diameter of the spray nozzle exceeds the diameter of the child's nostril. The limiting effects on nasal deposition due to the reduced airway dimensions in children result in an even greater challenge for efficient and reproducible nasal drug delivery in children compared to adults. In addition, the smaller volume capacity of the nasal vestibule in pediatric patients may result in significant anterior drainage of any nasally administered, liquid spray formulations that fail to pass through the nasal valve and instead deposit in the anterior/nostril region of the nasal cavity.

While this geometric model provides a simple and rapid method to predict maximal turbinate region deposition and minimal anterior/nostril region loss, additional advanced computational approaches using CFD can be used to further evaluate specific aspects of nasal deposition patterns in more detail. CFD models can incorporate individual human nasal cavity dimensions along with spray and user characteristics to simulate deposition patterns in individual users (9,16,29,30). For example, a study conducted by Keeler et al. used anatomically accurate CFD simulations to demonstrate that particle deposition patterns differed among subjects with different ethnicities based on the anatomical differences in their nasal cavities (30). Evaluating changes in user variables, such as user administration angles, or in spray characteristics, such as droplet velocities or non-homogenous spray plumes, are also handled better using CFD modeling, yet access to CFD software, appropriate MRI or CT-based images on which to develop the required CFD mesh for modeling, and software training time all limit the utility of CFD modeling for rapid formulation-device evaluations during preclinical nasal spray development. Although the geometric model described in this report does not incorporate the entire nasal airway anatomy, results from these simulations correlate well with experimentally determined deposition values (6,12) and to other reported CFD findings (2,9,16). Both model systems highlight the limiting effect of the nasal valve on any subsequent turbinate region deposition of sprayed formulations, yet the simplicity and limited need for computational resources makes the geometric model a simple yet effective tool for early-stage screening of nasal spray formulation and device combinations.

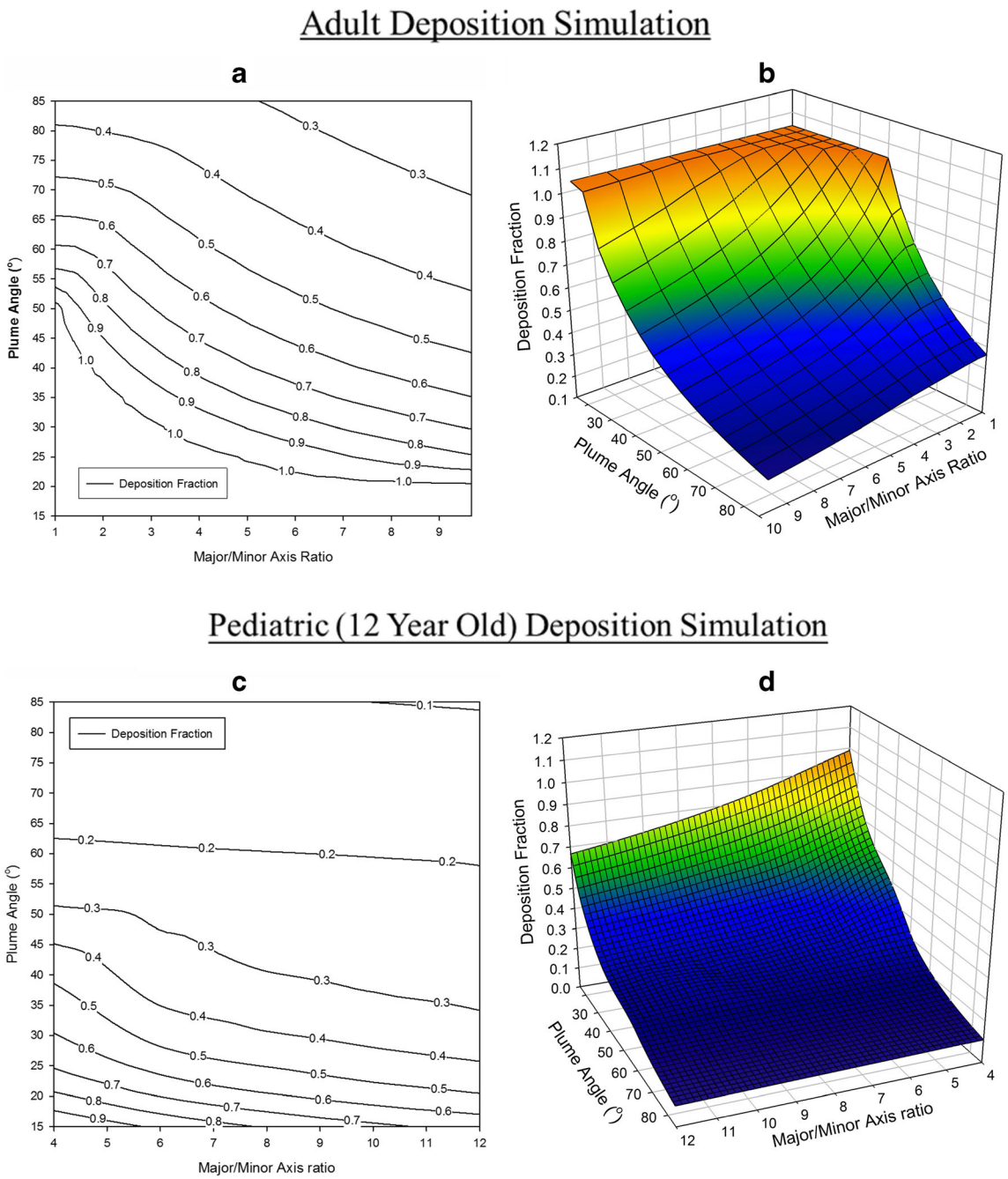

Fig. 5. Deposition efficiency simulations of nasal sprays with different plume angles passing through an elliptical shape nasal valve of fixed cross-sectional area with varying major/minor axis ratios. **a** *x-y* contour plot and **b** 3-D response surface plot for a fixed nasal valve cross-sectional area of 0.7 cm^2 representing nasal valve dimensions of an adult. **c** *x-y* contour plot and **d** 3-D response surface plot for a fixed nasal valve cross-sectional area of 0.2 cm^2 representing nasal valve dimensions of a child

CONCLUSIONS

This geometric model provides a simple method to quantitatively predict the effect of spray plume angle, spray administration distance, and nasal valve geometry on turbinate region deposition efficiency. It offers the opportunity to quickly identify lead formulations or to screen spray devices for efficient nasal deposition without the need to conduct extensive *in vitro* or *in vivo* deposition testing. The results obtained from simulations using the geometric model highlight the significant dependence of nasal deposition patterns on the dimensions of the nasal valve region, and the variation in size and shape of the nasal valve between nostrils and between patients is likely to contribute to the inter-patient

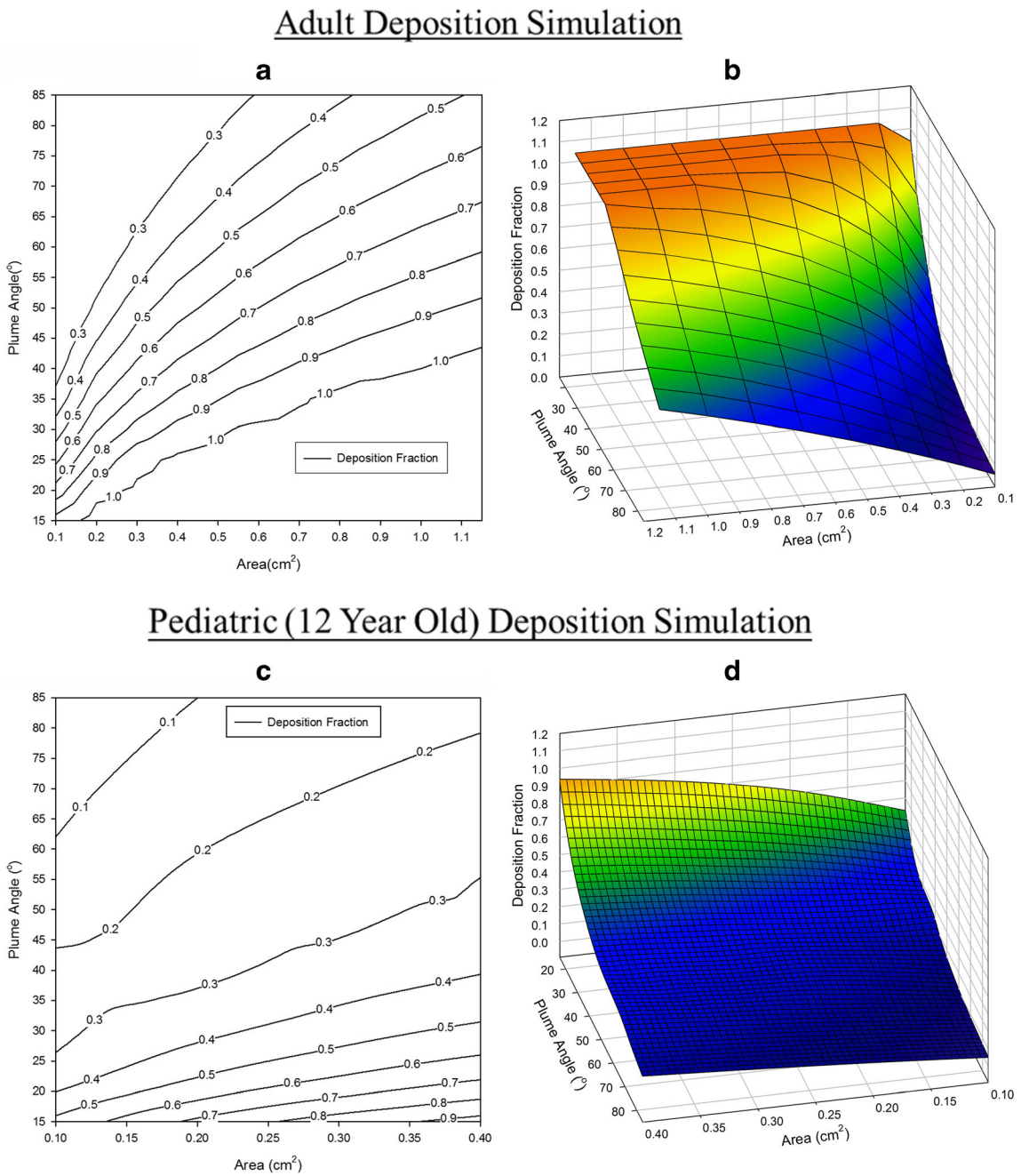

Fig. 6. Deposition efficiency simulations of nasal sprays with different plume angles passing through a nasal valve region with fixed major to minor axis ratio but varying cross-sectional area. **a** *x-y* contour plot and **b** 3-D response surface plot for a fixed major to minor axis ratio of 2.4 representing nasal valve dimensions of an adult. **c** *x-y* contour plot and **d** 3-D response surface plot for a fixed major to minor axis ratio of 10 representing dimensions of a 12-year-old child's nasal valve

variation frequently observed with nasal spray dosage forms. Even more significant differences in nasal valve dimensions observed among children of different ages are expected to lead to measurable differences in deposition in the pediatric population compared to adults. Further investigations of spray geometries able to maximize deposition efficiencies in children by using simulations with the simple geometric model will contribute significantly to the improved design of nasal spray delivery systems for children while reducing the need for extensive clinical testing to identify appropriate formulations and spray devices.

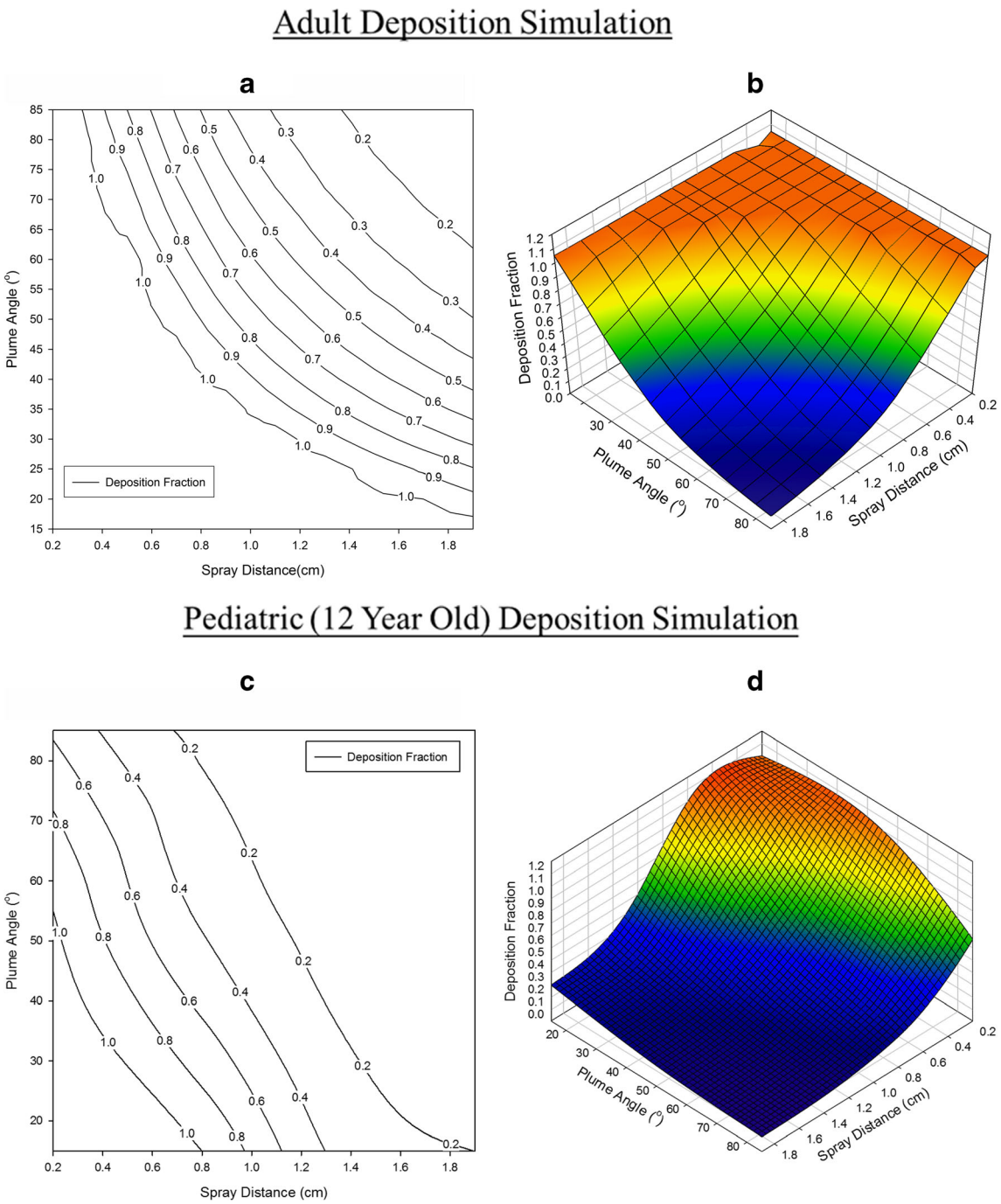

Fig. 7. Deposition efficiency simulations of sprays for various plume angles using a fixed nasal valve cross-sectional area and a fixed major to minor axis ratio while varying actuation distance from device tip to the nasal valve. **a** *x-y* contour plot and **b** 3-D response surface plot for a fixed nasal valve cross-sectional area (0.7 cm^2) and fixed major to minor axis ratio (2.4) representing dimensions of an adult nasal valve. **c** *x-y* contour plot and **d** 3-D response surface plot for a fixed nasal valve cross-sectional area (0.2 cm^2) and a fixed major to minor axis ratio (10) representing dimensions of a 12-year-old pediatric nasal valve

Funding Information This study was funded by an FDA Grant to the National Institute for Pharmaceutical Technology and Education (NIPTE) titled "The Critical Path Manufacturing Sector Research Initiative (U01)": grant no. 5U01FD004275.

The results and conclusions presented reflect the opinions of the authors and not those of the funding agencies.

REFERENCES

1. Cheng YS, Yeh HC, Swift DL. Aerosol deposition in human nasal airway for particles 1 nm to 20 μm: a model study. Radiat Prot Dosim. 1991;38:41–7.
2. Kimbell JS, Segal RA, Asgharian B, Wong BA, Schroeter JD, Southall JP, et al. Characterization of deposition from nasal spray devices using a computational fluid dynamics model of the human nasal passages. J Aerosol Med. 2007;20(1):59–74.
3. Frank DO, Kimbell JS, Pawar S, Rhee JS. Effects of anatomy and particle size on nasal sprays and nebulizers. Otolaryngol Head Neck Surg. 2012;146(2):313–9.
4. Xi J, Si X, Kim JW, Berlinski A. Simulation of airflow and aerosol deposition in the nasal cavity of a 5-year-old child. J Aerosol Sci. 2011;42(3):156–73.
5. Kundoor V, Dalby RN. Effect of formulation and administration related variables on deposition pattern of nasal spray pumps evaluated using a nasal cast. Pharm Res. 2011;28(8):1895–904.
6. Foo MY, Cheng YS, Su WC, Donovan MD. The influence of spray properties on intranasal deposition. J Aerosol Med. 2007;20(4):495–508.
7. Suman JD, Laube BL, Lin T, Brouet G, Dalby R. Validity of in vitro tests on aqueous spray pumps as surrogates for nasal deposition. Pharm Res. 2002;19(1):1–6.
8. Laube BL, Sharpless G, Vikani AR, Harrand V, Zinreich SJ, Sedberry K, et al. Intranasal deposition of Accuspray™ aerosol in anatomically correct models of 2-, 5-, and 12-year-old children. J Aerosol Med Pulm Drug Deliv. 2015;28(5):320–33.
9. Tong X, Dong J, Shang Y, Inthavong K, Tu J. Effects of nasal drug delivery device and its orientation on sprayed particle deposition in a realistic human nasal cavity. Comput Biol Med. 2016;77:40–8.
10. Newman SP, Moren F, Clarke SW. Deposition pattern of nasal sprays in man. Rhinology. 1988;26(2):111–20.
11. Xi J, Yuan JE, Zhang Y, Nevorski D, Wang Z, Zhou Y. Visualization and quantification of nasal and olfactory deposition in a sectional adult nasal airway cast. Pharm Res. 2016;33(6):1527–41.
12. Sawant NA, Donovan MD. In vitro assessment of spray deposition patterns in a pediatric (12 year-old) nasal cavity model. Pharm Res. 2018;35(5):108.
13. Kublik H, Vidgren MT. Nasal delivery systems and their effect on deposition and absorption. Adv Drug Deliv Rev. 1998;29(1):157–77.
14. Aggarwal R, Cardozo A, Homer J. The assessment of topical nasal drug distribution. Clin Otolaryngol. 2004;29(3):201–5.
15. Hallworth GW, Padfield JM. A comparison of the regional deposition in a model nose of a drug discharged from metered serosel and metered-pump nasal delivery systems. J Allergy Clin Immunol. 1986;77(2):348–53.
16. Inthavong K, Tian Z, Li H, Tu J, Yang W, Xue C, et al. A numerical study of spray particle deposition in a human nasal cavity. Aerosol Sci Technol. 2006;40(11):1034–45.
17. Rygg A, Hindle M, Longest PW. Linking suspension nasal spray drug deposition patterns to pharmacokinetic profiles: a proof-of-concept study using computational fluid dynamics. J Pharm Sci. 2016;105(6):1995–2004.
18. Engelhardt L, Röhm M, Mavoungou C, Schindowski K, Schafmeister A, Simon U. First steps to develop and validate a CFPD model in order to support the design of nose-to-brain delivered biopharmaceuticals. Pharm Res. 2016;33(6):1337–50.
19. Abd El-Shafy MA PJ, Bommareddy GSP, Dondeti P, Egbaria K. Plume geometry and spray pattern tests as tools to predict nasal deposition. AAPS PharmSci. 2000;2(2):Abstract 297. http://abstracts.aaps.org/SecureView/AAPSJournal/radzmy0fbng.htm
20. Foo MY. Deposition pattern of nasal sprays in the human nasal airway—interactions among formulation, device, anatomy and administration techniques: University of Iowa; 2007.
21. Larson RE, Hostetler RP, Edwards BH. Multiple integration. In: Calculus with analytical geometry. Lexington: D. C. Heath and Company; 1990. p. 959.
22. Gillett P. Calculus and analytic geometry. Lexington: D. C. Heath and Company; 1981. p. 641–5.
23. Xi J, Longest PW. Numerical predictions of submicrometer aerosol deposition in the nasal cavity using a novel drift flux approach. Int J Heat Mass Transf. 2008;51(23):5562–77.
24. Dastan A, Abouali O, Ahmadi G. CFD simulation of total and regional fiber deposition in human nasal cavities. J Aerosol Sci. 2014;69:132–49.
25. Kesavanathan J, Bascom R, Swift DL. The effect of nasal passage characteristics on particle deposition. J Aerosol Med. 1998;11(1):27–39.
26. Riechelmann H, Rheinheimer M, Wolfensberger M. Acoustic rhinometry in pre-school children. Clin Otolaryngol. 1993;18(4):272–7.
27. Pedersen O, Hilberg O, Berkowitz R, Yamagiwa M. Nasal cavity dimensions in the newborn measured by acoustic reflections. Laryngoscope. 1994;104(8):1023–8.
28. Warren D, Duany L, Fischer N. Nasal pathway resistance in normal and cleft lip and palate subjects. Cleft Palate Craniofac J. 1969;6:134–40.
29. Ghahramani E, Abouali O, Emdad H, Ahmadi G. Numerical analysis of stochastic dispersion of micro-particles in turbulent flows in a realistic model of human nasal/upper airway. J Aerosol Sci. 2014;67:188–206.
30. Keeler JA, Patki A, Woodard CR, Frank-Ito DO. A computational study of nasal spray deposition pattern in four ethnic groups. J Aerosol Med Pulm Drug Deliv. 2016;29(2):153–66.